Journal Name

ARTICLE TYPE

Cite this: DOI: 10.1039/xxxxxxxxxx

Improving the Activity of Gold Nanoparticles for the Water Gas Shift Reaction using TiO_2-Y_2O_3: an Example of Catalysts Design

Jose J. Plata,*[a] Francisca Romero-Sarria,[b] Javier Amaya Suárez,[a] Antonio M. Márquez,[a] Óscar H. Laguna,[b] José A. Odriozola,[b] and Javier Fdez. Sanz[a]

Received Date
Accepted Date

DOI: 10.1039/xxxxxxxxxx

www.rsc.org/journalname

In the last ten years, there has been an acceleration in the pace at which new catalysts for the water gas shift reaction are designed and synthesized. Pt-based catalysts remain the best solution when only activity is considered. However, cost, operation temperature, and deactivation phenomena are important variables when these catalysts are scaled in industry. Here, a new catalyst, Au/TiO_2-Y_2O_3 is presented as an alternative to the less selective Pt/oxide systems. Experimental and theoretical techniques are combined to design, synthesize, characterize and analyze the performance of this system. The mixed oxide produces a synergistic effect, improving the activity of the catalyst not only at large-medium temperatures but also at low temperatures. This effect is related to the homogeneous dispersion of the vacancies that act both as nucleation centers for smaller and more active gold nanoparticles and as dissociation sites for water molecules. Calculated reaction path points to the carboxyl formation as the rate-limiting step with an activation energy of $6.9\,\mathrm{kcal\,mol^{-1}}$, which is in quantitative agreement with experimental measurements and, to the best of our knowledge, it is the lowest activation energy reported for the water-gas shift reaction. This discovery demonstrates the importance of combining experimental and theoretical techniques to model and understand catalytic processes and opens the door to new improvements to reduce the operating temperature and the deactivation of the catalyst.

1 Introduction

The discovery of the catalytic activity of supported gold nanoparticles for the oxidation of CO can be considered a breakthrough in the development of environmental applied catalysis.[1–3] Gold nanoparticles present activity for many reactions such as propylene epoxidation, hydrochlorination, NO reduction or NO_2 decomposition,[4] however, CO oxidation,[5,6] and water-gas shift, WGS,[7–9] reaction stand as the two main applications for this system. During the last twenty years, different approaches have been explored to boost the activity of these supported catalysts for the WGS reaction. The nature of the metal[10–13] and the configuration of the catalyst[14,15] are the two most used routes. The substitution of gold by other metals such as Cu,[11] Pt,[12,13] or Ni[10,16] was recursively used as a method to explore the activity of new catalysts. Inverse configurations, in which the metal is used as the support for oxide nanoclusters, also produce very active catalysts when compared to others that were synthesized using conventional configurations.[15]

Although some studies present the effect of the oxide as indirect,[17] the bifuctional nature of the catalyst and the key role of the oxide has been confirmed.[18] While CO is preferentially adsorbed on the metallic centers, water dissociation takes place on the oxide. This bifunctional nature increases the difficulty in the design of new active catalysts. The catalyst should present not only both active centers but also optimize their distribution to minimize the transport phenomena between both sites. New configurations have been proposed following these design premises.[9,15] For instance, the adsorption of metallic clusters and CeO_x nano islands on TiO_2 produces highly active catalysts for the WGS reaction.[9,19]

The modification of the oxide surface has also been demonstrated as an effective strategy to increase the activity of other reactions that require a bifunctional catalyst such as the CO preferential oxidation, PROX. We have recently reported how Y doping on anatase TiO_2 modifies the surface creating vacancies.[20] These vacancies are homogeneously distributed on the surface and act as preferential adsorption sites for O_2 and nucleation centers for very small and well-dispersed gold nanoclusters.[21] The similarities between PROX and WGS reactions potentially make

[a] Departamento de Química Física, Universidad de Sevilla, Seville, Spain; E-mail: jplata@us.es
[b] Departamento de Química Inorgánica e Instituto de Ciencia de Materiales de Sevilla (ICMS), Centro mixto CSIC-Universidad de Sevilla, Seville, Spain.

the Au/TiO_2-Y_2O_3 system a good candidate for the WGS reaction, too.

2 Experimental and theoretical methods

2.1 Synthesis and characterization

The support was synthesized by a sol-gel method using titanium tert-butoxyde and yttrium nitrate as metallic precursors. A mixture of H_2O/NH_3 (28.5/1 ratio) and 1-buthanol were used as hydrolysis agent and the solvent respectively. The excess of solvent was eliminated by Soxhlet solid-liquid extraction and the solid was obtained by calcination at 573 K for 2 h. Gold, 1 wt%, was incorporated into the support by a deposition-precipitation (DP) using chloroauric acid (ALDRICH) as metallic source. The pH of the acid precursor solution was adjusted to 7 by adding NaOH 0.1 M. The support was added and the solution maintained at constant temperature at 353 K during 3 h. Finally, the solid was washed until Cl-disappearance, dried and calcined for 2 h at 573 K. A more detailed procedure of the synthesis and its characterisation has been reported in Ref. 21. The BET specific surface area of the samples was determined by N_2 adsorption at liquid nitrogen temperature in a Micromeritics ASAP 2010 apparatus. The degasification was carried out in vacuum at 423K for 2 hours. Dopant content was determined by X-ray fluorescence (XRF) using a Siemens SRS 3000 sequential spectrophotometer equipped with a rhodium tube onto pressed pellets obtaining a 11 wt.% of Y. X-Ray diffraction (XRD) patterns were recorded using a Siemens Kristalloflex D-501 diffractometer with Cu-Kα radiation (λ = 1.5404 Å) in continuous scan mode over a 2h-range of 20-80° using a step size of 0.05° and a step time of 1.0 s. TEM images were taken with a Talos F200S, equipped with a 200 kV S-FEG (high stability FEG emitter), as well as a condenser lens system with all automated apertures, analytical objective lens with contact power, automated objective aperture and HAADF STEM detector having a resolution of 0.25 nm.

2.2 Catalytic activity

The catalytic activity of the samples was analyzed in the low temperature WGS reaction over the 420-580 K range . The reaction was measured in a stainless steel tubular reactor with internal diameter of 9 mm and a height of 0.5 mm, for 0.5 g of the catalysts with a particle size between 0.4-0.5 mm. The activation of the catalysts was carried out in two steps. The first one with 50 mL min^{-1} total flow of 21% O_2 in N_2, heating from room temperature until 573K during 2 hours. Then, at the same temperature, a 50 mL min^{-1} total flow of 21% H_2 in N_2 was passed over the solid for 2 hours. This pre-treatment was designed to guarantee the removal of non-desired species by oxidation and the metallic state of the gold nanoparticles. For the reaction, a mixture of 3% CO, 67% N_2 (controlled by mass flow controllers) and 30% H_2O (controlled by a Gilson® 307 pump) in a total flow of 50 mL min^{-1}, was passed throughout the solid with a space velocity (SV) of 6000 $cm^3 g_{cat}^{-1} h^{-1}$. The temperature was increased from 433/443 K to 573 K in steps of 20 K. For each step, the temperature was stabilized and data were recorded at steady-state conditions. Online analyses of the feed and products streams were performed on a Varian® CP-4900 Micro Gas Chromatograph equipped with a Porapak Q a Molecular Sieve 5 Å and a TCD detector. The CO conversion, $\%CO_{conversion}$, during the WGS was calculated as

$$\%CO_{conversion} = \frac{(CO_{in} - CO_{out}) \cdot 100}{CO_{in}}, \quad (1)$$

where CO_{in} corresponds to CO volume in the inlet and CO_{out} represents the CO volume at the outlet. TOF was calculated as,

$$TOF = \frac{r_{CO} M_{Au}}{D_{Au}}, \quad (2)$$

where r_{CO} is the reaction rate in $mol_{CO\ converted}\ g_{Au}^{-1} s^{-1}$, M_{Au} is the atomic weigh of gold and D_{Au} is the gold dispersion that is estimated based on Au particle size measured by TEM and using an spherical model,

$$D_t(\%) = \frac{3 M_{Au} SF}{2 N_A R_{Au} \rho_{Au} \sigma} \cdot 100. \quad (3)$$

While SF is the stoichiometric factor, which is assumed as 1:1, N_A is the Avogadro's number, R_{Au} is the average radius of the Au nanoparticles, ρ_{Au} is the gold density and σ is the atomic cross-sectional area (0.0649 nm^2).[16]

2.3 Computational details

Periodic DFT calculations were carried out using the VASP code[22–24] and the projector augmented wave (PAW) method.[25,26] Energies were obtained using the generalized gradient approximation (GGA) implementation of DFT proposed by Perdew *et al.*[27] and a plane-wave basis set with a cutoff of 400 eV. In all cases, the Brillouin zone was sampled at the Γ point. Hellmann-Feyman theorem was used to calculate the forces over the ions including the Harris-Foulkes corrections.[28] Geometries were considered optimized when the forces over all atoms were less than 0.05 eV $Å^{-1}$. The transition states of three steps that usually determines the rate of the reaction: i) water dissociation, ii) carboxyl formation and iii) carboxyl decomposition,[29] were calculated using the climbing image version of the nudged elastic band, NEB, algorithm.[30] Vibrational analysis were performed for the transition states to ensure only one imaginary frequency. Anatase TiO_2 (101) slab models with two O-Ti-O trilayers and a 14 Å vacuum were used to describe the support (Figure 1). A 4×3 supercell in the [010] and $[10\bar{1}]$ directions was created to replicate the experimental doping load and the size predicted for gold nanoparticles. Eight Ti atoms were substituted by Y atoms creating 4 structural oxygen vacancies, O_v, used as nucleation center for the gold nanoparticle and the adsorption sites for four water molecules (Figure 1). The Y atoms were distributed following the most stable pattern increasing the Y content atom by atom. Y atoms are energetically favored at surface penta-coordinated positions (X_5c) compared with subsurface positions (X_6c) so atoms occupy these positions at low dopant loading. However, when the Y loading is increased, the most stable configurations correspond to arrangements in which half of the Y atoms are in X_6c sites in order to avoid Y-Y repulsions..[21] These vacancies, also homogeneously dispersed on

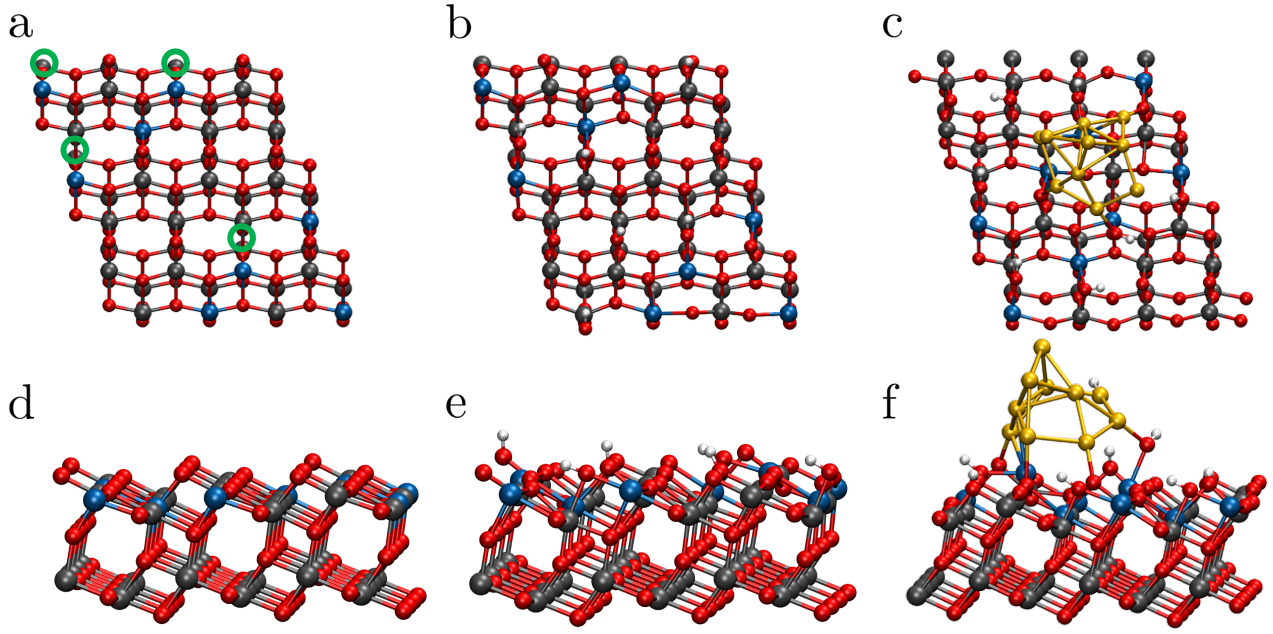

Fig. 1 Top and side view of the slab models: (a,d) clean doped surface, (b,e) hydroxylated doped surface, (c,f) hydroxylated doped surface with Au_{10} cluster. Green circles are located in O_v. Colors: Ti = gray, O = red, Y = blue, Au = yellow, and H = white.

the surface to stabilize the Y atoms,[21] are crucial to understand the nanoparticle dispersion and play an important role in the electronic properties of the gold clusters and its catalytic activity in the PROX reaction.[20] The Y:O_v ratio (2:1) was selected considering the vacancy formation energy of each O_v once all the Y atoms were substituted. Removing oxygen atoms from this model after Y-doping turns to be an exothermic process, and actually even the fourth O removal, which is the one that gives the correct stoichiometry, releases 0.08 eV. No electrons are localise in Ti 3d sates at this Y:O_v ratio. Thus no significative changes are expected between the use of a pure GGA functional or the inclusion of a Hubbard term to improve the electron localisation. A large Au_{10} nanoparticle, with a similar size to previous experimentally synthesized nanoparticles,[31] was adsorbed on the surface. The cluster was adsorbed atom by atom in order to model correctly the gold-surface interaction and its 3D growth on the surface. More details about the surface model can be obtained in Refs. 20 and 21.

3 Results

The catalytic activity for Au/TiO_2, Au/Y_2O_3 and Au/TiO_2-Y_2O_3 was measured in a range of temperature between 433 K and 573 K (Figure 2 a). The Au/TiO_2 system is used as a reference to evaluate the activity of the other two samples. For instance, while the Au/TiO_2 sample is only active above 500 K, the Au/Y_2O_3 catalyst shows activity even below 440 K. However, the most interesting results are obtained for the Au/TiO_2-Y_2O_3 samples. Au/TiO_2-Y_2O_3 catalyst duplicates the CO conversion of Au/Y_2O_3 samples at 573 K. Thus, a synergistic effect between both oxides that boosts the activity of the catalyst can be deduced from these data.

Activation energies were calculated at low conversions to study only the intrinsic reaction mechanism avoiding diffusion contributions (Figure 2 b). Au/TiO_2 samples present an apparent activation energy of 15.5 kcal mol^{-1}, which is slightly higher that the reported by other authors for rutile TiO_2, $10.0-14.3$ mol^{-1}.[17,32,33] To the best of our knowledge, there are no experimental measurements of the activity of the Au/Y_2O_3 system. However, its E_a, 8.6 kcal mol^{-1}, is close to the values reported for other oxides such as CeO_2, 8 kcal mol^{-1}.[34] Au/TiO_2-Y_2O_3 catalyst shows even a smaller barrier, 6.9 kcal mol^{-1}, which is below one of the most active gold-based catalyst, Au/CeO_x/TiO_2, whose E_a is 7 kcal mol^{-1}. Actually, activation energies above 6.9 kcal mol^{-1} have been reported for less selective,[35] more expensive but also highly active Pt-based catalyst.[36–38]

Although the activation energy for the TiO_2-Y_2O_3 system is quite low compared to TiO_2, the small difference with respect to the activation energy for the Au/Y_2O_3 samples cannot entirely explain the higher activity of the Au/TiO_2-Y_2O_3 catalyst. In a previous study, we addressed the high activity of this system for the PROX reaction as an effect of the redispersion of the gold nanoparticles.[20] TEM images were used to compare the distribution and size of the metal over the support (Figure 3 a). A reduction of more than a 50% in the average size of the gold nanoparticles is observed comparing the size distribution (Figure 3 b) on the TiO_2-Y_2O_3 support (8.0 nm) with respect to the Au/TiO_2 and Au/Y_2O_3 samples (18.3 nm and 21.7 nm respectively). Additionally, XRD patterns for the TiO_2-Y_2O_3 oxide only present anatase reflections with no apparent displacements with respect to the anatase peaks in the TiO_2 samples (Figure 4). These patterns suggest the predominant presence of well dispersed Y atoms on the surface of the oxide with no crystalline domain, which is in agreement with TEM images. The combination of XRD patterns and TEM images with previous DFT results[20] demonstrates the importance of the homogeneous distribution of Y on the surface

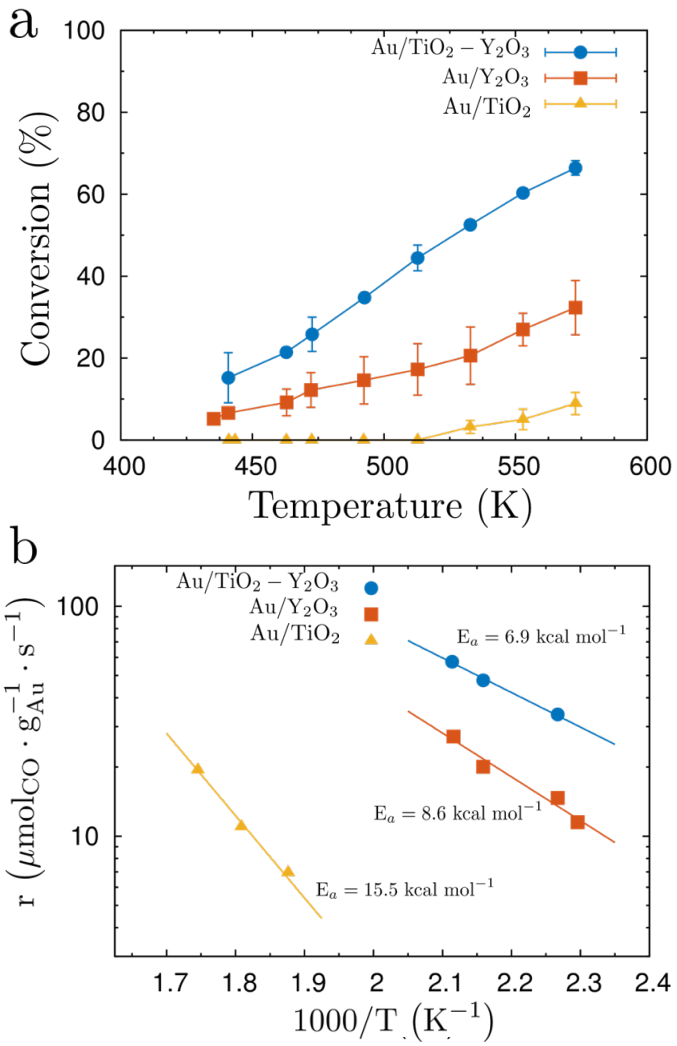

Fig. 2 a) CO conversion for Au/TiO_2 (yellow), Au/Y_2O_3 (orange) and Au/TiO_2-Y_2O_3 (blue) catalysts. b) Arrhenius plot for Au/TiO_2 (yellow), Au/Y_2O_3 (orange) and Au/TiO_2-Y_2O_3 (blue) catalysts.

of the oxide creating well-dispersed vacancies and producing the dispersion and size reduction of the gold nanoparticles. This finding represent another of the advantages of the TiO_2-Y_2O_3 support compare to TiO_2 . While very specific protocols or more expensive techniques are mandatory to reduces the gold nanoparticle average size and boost the activity on TiO_2, very small gold nanoparticles are directly obtained with a fast and inexpensive method such as DP on the TiO_2-Y_2O_3 oxide. The smaller the nanoparticles, the higher the percentage of under-coordinated gold atoms at the perimeter of the gold-oxide interface. These atoms are the most active centers for the CO oxidation because of the bifunctional nature of the catalyst. CO have to be adsorbed at the perimeter of the nanoparticle to react with the hydroxyl groups on the surface of the oxide. Moreover, while the reported competition between the gold and water for the vacancies was not critical for the PROX reaction,[20] the presence of water molecules around the vacancies and next to the nanoparticles creates a reservoir of hydroxyl groups for the reaction close to the active centers that is crucial in the case of the WGS reaction.

In addition to the extremely low activation energy, the Au/TiO_2-Y_2O_3 samples present high reaction rates and turn over frequencies, TOF. A TOF of 0.3 s^{-1} was obtained for the Au/TiO_2-Y_2O_3 samples at 573 K. There is a extensive literature reporting TOFs for the WGS reaction using supported gold nanoparticles as active centers (Table 1). Several authors have reported values ranging from $5.6 \cdot 10^{-5}$ to 3.8 s^{-1} for Au/TiO_2,[33,39–41] 3.9 s^{-1} on Au/CeO_2,[42] and up to 11 s^{-1} for $Au/CeO_x/TiO_2$.[41] Although TOF values are normalized by the amount of active centers, there are many operating variables such as temperature, pressure, contact time, spatial velocity, conversion, or reactants proportion in the gas mixture that make the comparison of different studies a difficult task. In this case, our TOF values are within the range of others gold-titania catalysts.[33,39–41] Recently, Ma *et al.* have reported the catalytic activity of $Au/M_xO_y/TiO_2$ systems using similar operating parameters to the ones used in this work.[43] The reaction rates are compared in Fig 5. Our Au/TiO_2-Y_2O_3 catalyst is not only approximately 10 times more active than the Au/TiO_2 catalyst– but also, when compared with other promoters such as holmium, being less expensive and more abundant.

Atomistic models were combined with DFT calculations to rationalize and understand the origin of the extraordinary low activation energy. Because of the bifunctional nature of the catalyst, both water dissociation and CO activation were studied. Water molecules are preferentially adsorbed on the structural vacancies of the surface,[21] presenting an adsorption energy, E_{ads}, around −26.5 kcal mol^{-1} (Figure 6 a). This value stands out when it is compared with other adsorption sites on the surface, at least 10.5 kcal mol^{-1} less stable than the vacancy site. The differences between the vacancy as adsorption site and other surface sites increase when the thermochemistry of the water dissociation is considered. While water dissociation is exothermic at the vacancy by −9.0 kcal mol^{-1}, the process is endothermic by 6.7 kcal mol^{-1} at other sites of the surface. CI-NEB calculations were carried out to quantify the activation energy for the water dissociation at the vacancy but the process takes place with no apparent barrier. This finding shows that there should be an important hydroxyl reservoir next to the nanoparticles with respect to other surfaces where water dissociation presents higher barriers such as rutile TiO_2[46] (0.32 eV), anatase TiO_2[47,48] (0.14-0.24 eV) or CeO_x/TiO_2[49] (0.04 eV).

In a previous study, we reported that the adsorption of the CO molecule takes place in edges and corners of the gold cluster, close to the interface with the surface.[20] For this reason, this section focuses on the oxidation of the adsorbed CO molecules with the dissociated water molecules. Near-ambient-pressure X-ray photoelectron spectroscopy (NAP-XPS) and infrared reflection absorption spectroscopy (IRRAS) measurements have demonstrated that for metal-oxide catalysts, the reaction takes places at the interface between both components via a carboxyl intermediate.[18,32] We found here that the carboxyl formation is an exothermic reaction by 9.0 kcal mol^{-1} with a moderate barrier of 6.9 kcal mol^{-1} (Figure 6 b,c). The deprotonation of the carboxyl intermediate presents an even lower activation energy, 5.1 kcal mol^{-1}, and it is considered almost thermoneutral. Despite the high stabilization of the CO_2 intermediate on the surface, it should be noticed

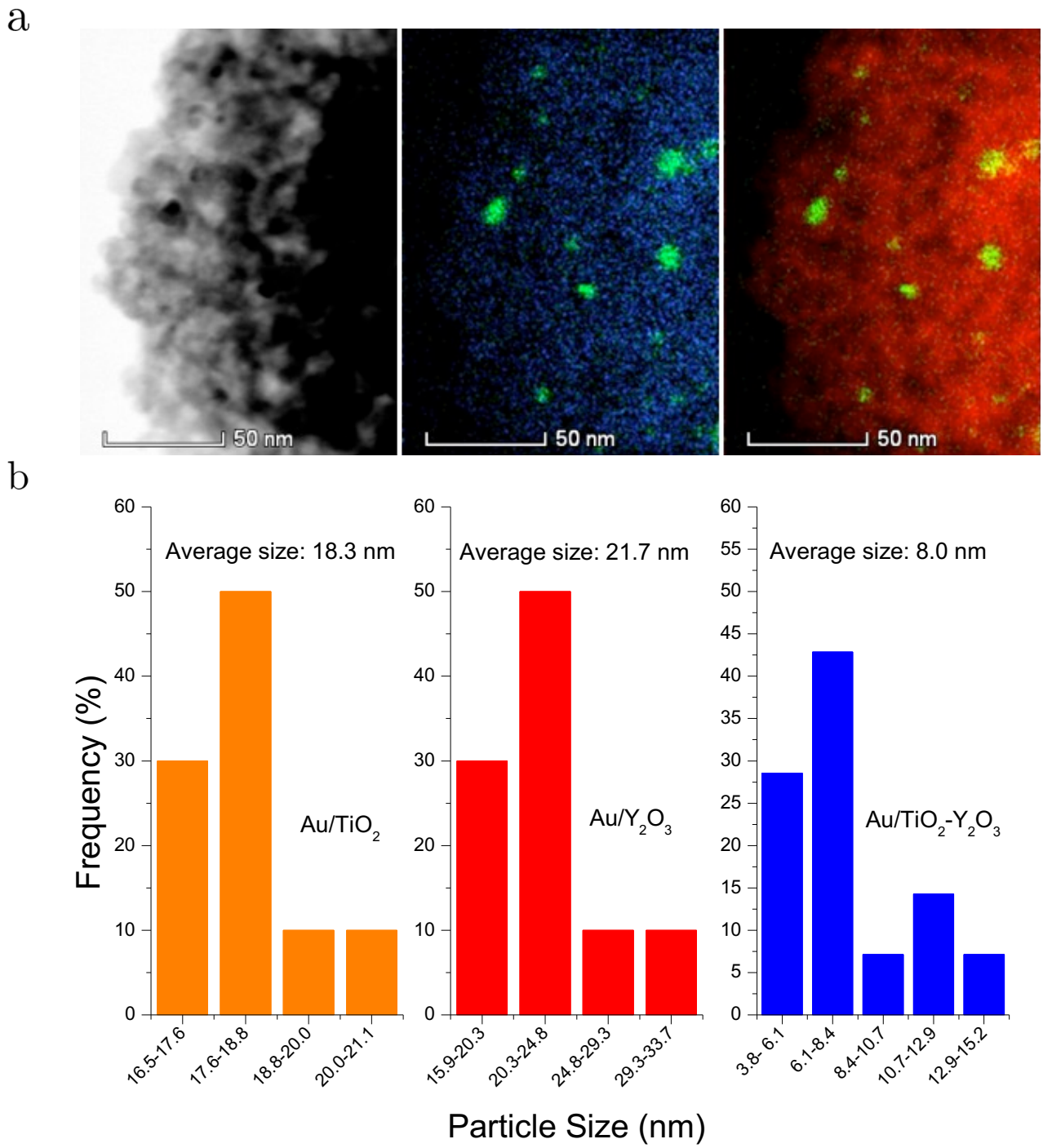

Fig. 3 a) Selected TEM images of the Au/TiO_2-Y_2O_3 samples. Colors: Au = green, Y = blue and Ti = red. b) Gold nanoparticle size distribution for Au/TiO_2, Au/Y_2O_3 and Au/TiO_2-Y_2O_3.

that the energy values reported at the products label in Figure 6 do not include desorption entropy contributions for CO_2 and H_2, that amount for 16.82 kcal mol^{-}1 and 13.10 kcal mol^{-1}, respectively at 625 K.[19] Therefore, carboxyl formation remains as the rate-limiting step of the catalytic cycle. The experimental apparent activation energy, which can be used as a good approximation for the rate-limiting step, is in agreement with this theoretical prediction.

4 Conclusions

A combined theoretical and experimental study was carried out to design highly active gold-based catalyst for the WGS reaction. Au/TiO_2, Au/Y_2O_3, and Au/TiO_2-Y_2O_3 samples were synthesized and characterized. The mixed oxide support produces a synergistic effect reducing the size of the gold nanoparticles and boosting the catalytic activity of the Au/TiO_2-Y_2O_3 sample. High TOFs and rates are obtained and compared with other studies with

Table 1 Comparison of WGS activity of Au-metal oxide catalysts. Units: temperature, T, in K, CO conversion, X_{CO}, in %, space velocity, SV, in $cm^3 g_{cat}^{-1} h^{-1}$, turn over frequency, TOF, in s^{-1}.

Sample	Au wt.%	T	% CO	% H_2O	% H_2	X_{CO}	SV	TOF
Au/TiO_2-Y_2O_3	1	573	3	30		70	6000	$3.0 \cdot 10^{-1}$
Au/TiO_2 [40] (WGC)[a]	1.57	573	4.76	35.38	28.46	52	15000	$1.3 \cdot 10^{-1}$
Au/TiO_2 [40] (DP)[b]	2.36	573	4.76	35.38	28.46	85	15000	$1.6 \cdot 10^{-1}$
Au/TiO_2 [40] (LPRD)[c]	1.38	573	4.76	35.38	28.46	70	15000	$1.8 \cdot 10^{-1}$
Au/TiO_2 [33]	2.3	393	6.8	11.0	37.4	10	30000	$1.5 \cdot 10^{0}$
Au/TiO_2 [39] (DP)[b]	7.9	373	1.0	2.0		<20	12600	$9.2 \cdot 10^{-4}$
Au/TiO_2 [39] (Cop)[d]	21.4	373	1.0	2.0		<20	12600	$5.6 \cdot 10^{-5}$
Au/Fe_2O_3 [39] (Cop)[d]	6.1	373	1.0	2.0		<20	12600	$9.1 \cdot 10^{-5}$
Au/Al_2O_3 [39] (Cop)[d]	9.2	373	1.0	2.0		<20	12600	$1.1 \cdot 10^{-4}$
Au/ZnO [39] (Cop)[d]	11.2	373	1.0	2.0		<20	12600	$5.7 \cdot 10^{-5}$
$Au/CeO_x/TiO_2$ [41]		625	66.66	33.33				$1.1 \cdot 10^{1}$
$Au/CeO_x/TiO_2$ [41]		625	66.66	33.33				$6.5 \cdot 10^{0}$
Au/TiO_2 [41]		625	66.66	33.33				$3.8 \cdot 10^{0}$
Au/CeO_2 [42]	4.79	513	12.0	22.0	43.0	90		$3.0 \cdot 10^{-1}$
Au/CeO_2 [42]	3.30	513	12.0	22.0	43.0	90		$3.9 \cdot 10^{0}$
Au/CeO_2 (La) [44]	0.57	573	11.0	26.0	26.0	80	90000	$1 \cdot 10^{0}$
Au/CeO_2-ZnO/Al_2O_3 [45]	1.99	523	4.5	30		65	8000	$4.3 \cdot 10^{-2}$

[a] WGC, world gold council.
[b] DP, depositionâĂŞprecipitation.
[c] LPRD, liquid phase reductive deposition.
[d] Cop, coprecipitation.

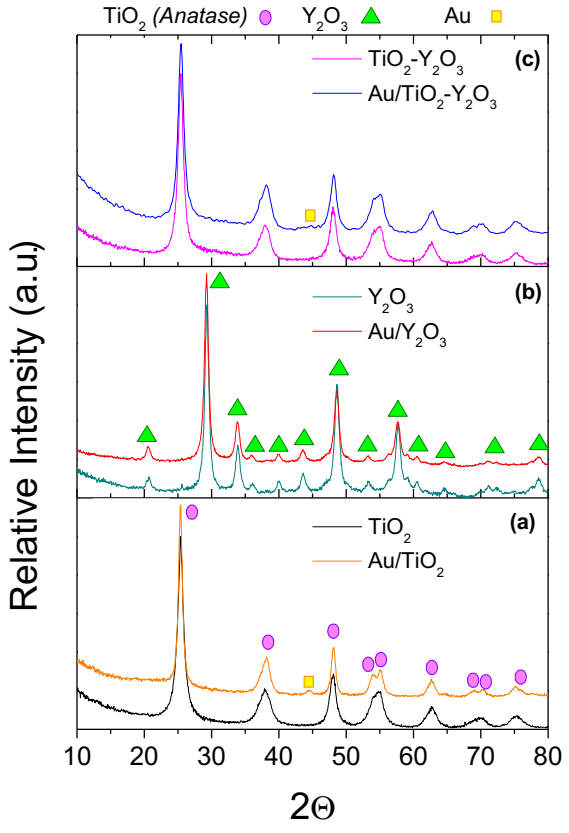

Fig. 4 XRD patterns for Au/TiO_2, Au/Y_2O_3 and Au/TiO_2-Y_2O_3 samples.

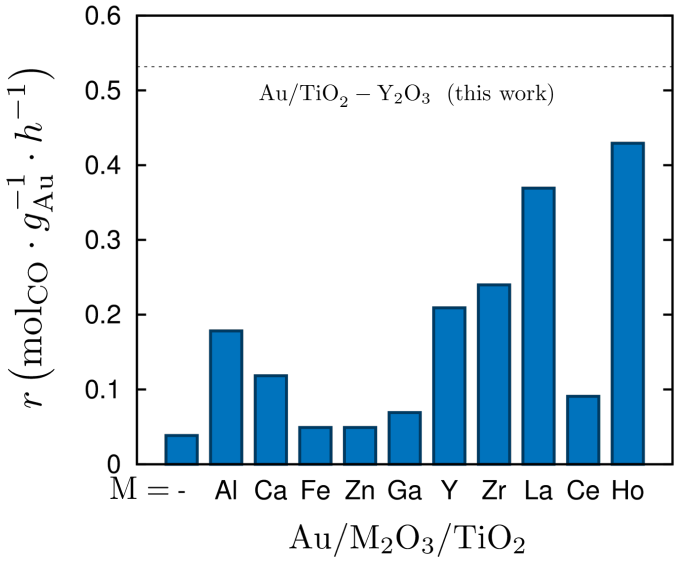

Fig. 5 Effect of M_xO_y modifiers on the catalytic performance of $Au/M_xO_y/TiO_2$ catalysts [43] compared to the rate for Au/TiO_2-Y_2O_3 (dashed line) at 573 K for the WGS reaction.

more expensive and scarce promoters. But even more important, an apparent activation energy of 6.9 kcal mol^{-1} is found for the Au/TiO_2-Y_2O_3 catalyst. To the best of our knowledge, this is the lowest activation barrier reported for the WGS reaction. DFT calculations were performed to explore the energy profile of the reaction. Our results demonstrate the importance of the vacancies not only as nucleation centers for the homogeneous dispersion of the gold atoms but also as preferential adsorption and dissociation sites for the water molecules. The apparent no barrier dissociation of water results in a reservoir of hydroxyl groups around the gold clusters which are available for the formation or carboxyl intermediates in the CO oxidation process. The calculated reaction profile points the carboxyl formation as the rate-limiting step of the reaction with an activation energy of 6.9 kcal mol^{-1}. This barrier is in good agreement with the experimental apparent activation energy obtained for Arrhenius plot. The reduction of the activation energy and nanoparticle size, increasing the number of active centers, opens the door to the design and synthesis of

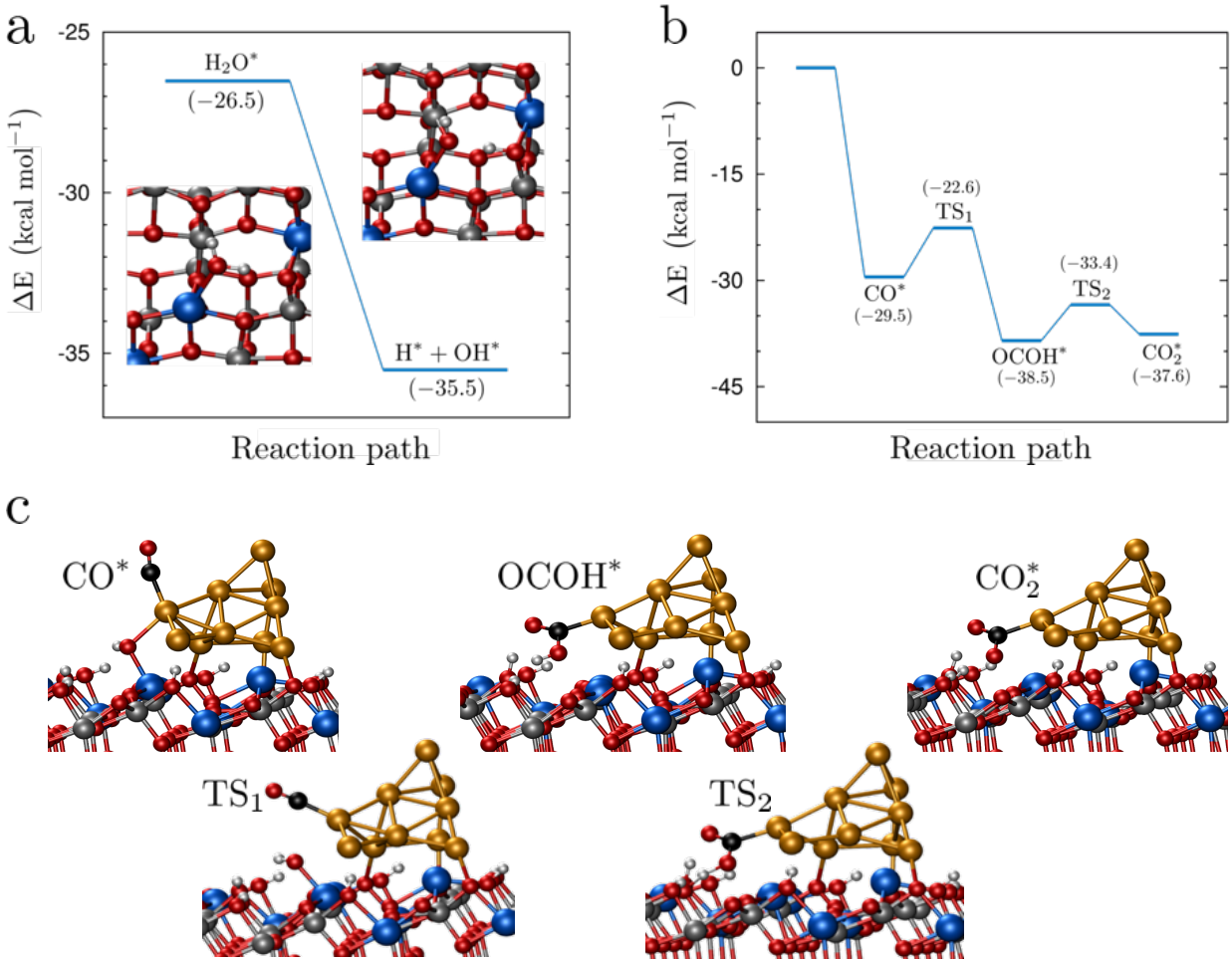

Fig. 6 a) Reaction path for the water dissociation at a surface vacancy. b) Reaction profile for the CO oxidation in the WGS reaction. c) Atomistic models of the most important intermediates and transition states, TS_x, of the reaction path. Colors: Ti = gray, O = red, Y = blue, Au = yellow, C = black, H = white.

other catalysts. This new approach can be combined with the use of cheaper metals such as Cu [19] or the addition of ionic conductors, [50,51] obtaining catalysts with higher conversions that can be very active at lower temperatures, reducing the common deactivation processes that these catalysts present at higher temperatures.

Conflicts of interest

There are no conflicts to declare.

Acknowledgements

This work was funded by the Ministerio de Economía y Competitividad (Spain, grants CTQ2015-64669-P and ENE2015-66975-C3-2-R) and European FEDER. The authors also acknowledge Junta de Andalucía for the financial support (grants FQM-132 and TEP-106). J.J.P. thanks Universidad de Sevilla for post-doctoral fellowship and and European Union?s Horizon 2020 research and innovation programme under the Marie Sk?odowska-Curie grant agreement HT-PHOTO-DB No 752608.

Notes and references

1 M. Haruta, *Catal. Today*, 1997, **36**, 153–166.
2 T. Hayashi, K. Tanaka and M. Haruta, *J. Catal.*, 1998, **178**, 566–575.
3 M. Haruta, *CATTECH*, 2002, **6**, 102–115.
4 M. Haruta, *Gold Bull.*, 2004, **37**, 27–36.
5 M. Kahlich, H. Gasteiger and R. Behm, *J. Catal.*, 1999, **182**, 430–440.
6 T. Choudhary and D. Goodman, *Top. Catal.*, 2002, **21**, 25–34.
7 Q. Fu, W. Deng, H. Saltsburg and M. Flytzani-Stephanopoulos, *Appl. Catal. B-Environ.*, 2005, **56**, 57–68.
8 Z.-P. Liu, S. Jenkins and D. King, *Phys. Rev. Lett.*, 2005, **94**, 19.
9 J. Rodríguez, S. Ma, P. Liu, J. Hrbek, J. Evans and M. Pérez, *Science*, 2007, **318**, 1757–1760.
10 Y. Li, Q. Fu and M. Flytzani-Stephanopoulos, *Appl. Catal. B-Environ.*, 2000, **27**, 179–191.
11 X. Wang, J. Rodríguez, J. Hanson, D. Gamarra, A. Martínez-Arias and M. Fernández-García, *J. Phys. Chem. B*, 2006, **110**, 428–434.
12 Y. Zhai, D. Pierre, R. Si, W. Deng, P. Ferrin, A. Nilekar, G. Peng, J. Herron, D. Bell, H. Saltsburg, M. Mavrikakis and M. Flytzani-Stephanopoulos, *Science*, 2010, **329**, 1633–1636.

13 A. Bruix, J. Rodríguez, P. Ramírez, S. Senanayake, J. Evans, J. Park, D. Stacchiola, P. Liu, J. Hrbek and F. Illas, *J. Am. Chem. Soc.*, 2012, **134**, 8968–8974.

14 J. Graciani and J. F. Sanz, *Catal. Today*, 2015, **240**, 214 – 219.

15 J. A. Rodríguez, P. Liu, J. Graciani, S. D. Senanayake, D. C. Grinter, D. Stacchiola, J. Hrbek and J. Fernández-Sanz, *J. Phys. Chem. Lett.*, 2016, **7**, 2627–2639.

16 M. Xu, S. He, H. Chen, G. Cui, L. Zheng, B. Wang and M. Wei, *ACS Catal.*, 2017, **7**, 7600–7609.

17 M. Flytzani-Stephanopoulos, *Accounts Chem. Res.*, 2014, **47**, 783–792.

18 K. Mudiyanselage, S. D. Senanayake, L. Feria, S. Kundu, A. E. Baber, J. Graciani, A. B. Vidal, S. Agnoli, J. Evans, R. Chang, S. Axnanda, Z. Liu, J. F. Sanz, P. Liu, J. A. Rodriguez and D. J. Stacchiola, *Angew. Chem. Int. Ed.*, 2013, **52**, 5101–5105.

19 J. J. Plata, J. Graciani, J. Evans, J. A. Rodríguez and J. F. Sanz, *ACS Catal.*, 2016, **6**, 4608–4615.

20 F. Romero-Sarria, J. Plata, O. Laguna, A. Márquez, M. Centeno, J. Sanz and J. Odriozola, *RSC Adv.*, 2014, **4**, 13145–13152.

21 J. Plata, A. Márquez, J. Sanz, R. Avellaneda, F. Romero-Sarria, M. Domínguez, M. Centeno and J. Odriozola, *Top. Catal.*, 2011, **54**, 219–228.

22 G. Kresse and J. Furthmüller, *Phys. Rev. B*, 1996, **54**, 11169–11186.

23 G. Kresse and J. Furthmüller, *Comput. Mater. Sci.*, 1996, **6**, 15–50.

24 G. Kresse and J. Hafner, *Phys. Rev. B*, 1993, **47**, 558–561.

25 G. Kresse and D. Joubert, *Phys. Rev. B*, 1999, **59**, 1758–1775.

26 P. Blöchl, *Phys. Rev. B*, 1994, **50**, 17953–17979.

27 J. P. Perdew, J. A. Chevary, S. H. Vosko, K. A. Jackson, M. R. Pederson, D. J. Singh and C. Fiolhais, *Phys. Rev. B*, 1992, **46**, 6671–6687.

28 J. Harris, *Phys. Rev. B*, 1985, **31**, 1770–1779.

29 A. A. Gokhale, J. A. Dumesic and M. Mavrikakis, *J. Am. Chem. Soc.*, 2008, **130**, 1402–1414.

30 G. Henkelman, A. Arnaldsson and H. Jónsson, *Comp. Mat. Sci.*, 2006, **36**, 354 – 360.

31 S. C. Chan and M. A. Barteau, *Langmuir*, 2005, **21**, 5588–5595.

32 J. A. Rodríguez, J. Evans, J. Graciani, J.-B. Park, P. Liu, J. Hrbek and J. F. Sanz, *J. Phys. Chem. C*, 2009, **113**, 7364–7370.

33 M. Shekhar, J. Wang, W.-S. Lee, M. C. Akatay, E. A. Stach, W. N. Delgass and F. H. Ribeiro, *J. Catal.*, 2012, **293**, 94 – 102.

34 J. Rodríguez, P. Liu, J. Hrbek, J. Evans and M. Pérez, *Angew. Chem. Int. Edit.*, 2007, **46**, 1329–1332.

35 C. M. Y. Yeung, K. M. K. Yu, Q. J. Fu, D. Thompsett, M. I. Petch and S. C. Tsang, *J. Am. Chem. Soc.*, 2005, **127**, 18010–18011.

36 D. Miao, A. Goldbach and H. Xu, *ACS Catal.*, 2016, **6**, 775–783.

37 C. Sener, T. Wesley, A. Alba-Rubio, M. Kumbhalkar, S. Hakim, F. Ribeiro, J. Miller and J. Dumesic, *ACS Catal.*, 2016, **6**, 1334–1344.

38 A. Duke, K. Xie, A. Brandt, T. Maddumapatabandi, S. Ammal, A. Heyden, J. Monnier and D. Chen, *ACS Catal.*, 2017, **7**, 2597–2606.

39 H. Sakurai, A. Ueda, T. Kobayashi and M. Haruta, *Chem. Commun.*, 1997, 71–272.

40 P. Pérez, M. A. Soria, S. A. Carabineiro, F. J. Maldonado-Hódar, A. Mendes and L. M. Madeira, *Int. J. Hydrog. Energy*, 2016, **41**, 4670 – 4681.

41 D. Grinter, J. Park, S. Agnoli, J. Evans, J. Hrbek, D. Stacchiola, S. Senanayake and J. Rodriguez, *Surf. Sci.*, 2016, **650**, 34 – 39.

42 C. H. Kim and L. T. Thompson, *J. Catal.*, 2005, **230**, 66 – 74.

43 Z. Ma, H. Yin and S. Dai, *Catal. Lett.*, 2010, **136**, 83.

44 W. Deng, C. Carpenter, N. Yi and M. Flytzani-Stephanopoulos, *Top. Catal.*, 2007, **44**, 199.

45 T. R. Reina, S. Ivanova, J. J. Delgado, I. Ivanov, V. Idakiev, T. Tabakova, M. A. Centeno and J. A. Odriozola, *ChemCatChem*, 2014, **6**, 1401–1409.

46 J. Oviedo, R. Sánchez-de Armas, M. A. San Miguel and J. F. Sanz, *J. Phys. Chem. C*, 2008, **112**, 17737–17740.

47 U. Aschauer, Y. He, H. Cheng, S.-C. Li, U. Diebold and A. Selloni, *J. Phys. Chem. C*, 2010, **114**, 1278–1284.

48 A. Tilocca and A. Selloni, *J. Phys. Chem. C*, 2012, **116**, 9114–9121.

49 J. Graciani, J. J. Plata, J. F. Sanz, P. Liu and J. A. Rodriguez, *J. Chem. Phys.*, 2010, **132**, 104703.

50 M. G.-C. no, S. Ivanova, O. Laguna, L. M. T., M. Centeno and J. Odriozola, *Appl. Catal. B-Environ.*, 2017, **200**, 420 – 427.

51 N. Garcia-Moncada, M. G.-C. no, S. Ivanova, M. ÃĄngel Centeno, F. Romero-Sarria and J. A. Odriozola, *Appl. Catal. B-Environ.*, 2018, **238**, 1 – 5.